Chemical Science

ROYAL SOCIETY OF CHEMISTRY

EDGE ARTICLE

View Article Online
View Journal | View Issue

Cite this: *Chem. Sci.*, 2021, **12**, 12939

All publication charges for this article have been paid for by the Royal Society of Chemistry

Received 13th July 2021
Accepted 24th August 2021

DOI: 10.1039/d1sc03828a

rsc.li/chemical-science

Leveraging an enzyme/artificial substrate system to enhance cellular persulfides and mitigate neuroinflammation†

Prerona Bora, ‡[a] Suman Manna, ‡[a] Mrutyunjay A. Nair, ‡§[a] Rupali R. M. Sathe,[b] Shubham Singh,[b] Venkata Sai Sreyas Adury,[a] Kavya Gupta,[c] Arnab Mukherjee,[a] Deepak K. Saini,[c] Siddhesh S. Kamat,[b] Amrita B. Hazra *[ab] and Harinath Chakrapani *[a]

Persulfides and polysulfides, collectively known as the sulfane sulfur pool along with hydrogen sulfide (H_2S), play a central role in cellular physiology and disease. Exogenously enhancing these species in cells is an emerging therapeutic paradigm for mitigating oxidative stress and inflammation that are associated with several diseases. In this study, we present a unique approach of using the cell's own enzyme machinery coupled with an array of artificial substrates to enhance the cellular sulfane sulfur pool. We report the synthesis and validation of artificial/unnatural substrates specific for 3-mercaptopyruvate sulfurtransferase (3-MST), an important enzyme that contributes to sulfur trafficking in cells. We demonstrate that these artificial substrates generate persulfides *in vitro* as well as mediate sulfur transfer to low molecular weight thiols and to cysteine-containing proteins. A nearly 100-fold difference in the rates of H_2S production for the various substrates is observed supporting the tunability of persulfide generation by the 3-MST enzyme/artificial substrate system. Next, we show that the substrate **1a** permeates cells and is selectively turned over by 3-MST to generate 3-MST-persulfide, which protects against reactive oxygen species-induced lethality. Lastly, in a mouse model, **1a** is found to significantly mitigate neuroinflammation in the brain tissue. Together, the approach that we have developed allows for the on-demand generation of persulfides *in vitro* and *in vivo* using a range of shelf-stable, artificial substrates of 3-MST, while opening up possibilities of harnessing these molecules for therapeutic applications.

Introduction

Hydrogen sulfide (H_2S) and its redox congeners, persulfides (HSSH) and polysulfides (H_2S_n) act as mediators of several intracellular signaling processes.[1,2] Persulfides and polysulfides, collectively known as the sulfane sulfur pool, along with H_2S are summoned in response to oxidative stress in cells, and dysfunctional sulfur metabolism is implicated in neurodegeneration,[3,4] cardiovascular disease[5,6] and antibiotic resistance.[7,8] To regulate the sulfane sulfur pool, one of the strategies used by cells is to employ protein persulfidation, a post-translational modification where the thiol group of a reactive cysteine (Cys-SH) is modified to a persulfide (Cys-SSH).[9] The persulfidated protein mediates S-transfer to appropriate biomolecular targets, and not only provides protection against irreversible oxidation of cysteine residues but also regulates cellular signaling and sulfur homeostasis.[10,11] Persulfidation has been linked to modulation of the catalytic activity of key proteins such as parkin and GSK-3β that are involved in neurodegenerative diseases, underscoring the therapeutic relevance of exogenously controlling this post-translational modification by administering persulfide/H_2S.[4,9] Here, we report a novel approach of developing artificial/unnatural substrates for persulfide-generating enzymes *in vivo* as a tool to study and tune sulfur metabolism in cells with applications in mitigating neuroinflammation.

In this study, we leverage natural biochemical mechanisms for generating persulfides by the development of a new class of substrates for 3-mercaptopyruvate sulfurtransferase (3-MST), a central persulfide/polysulfide generating enzyme that has been implicated in the mitigation of oxidative stress.[12–14] 3-MST

[a]*Department of Chemistry, Indian Institute of Science Education and Research Pune, Dr. Homi Bhabha Road, Pashan, Pune 411 008, Maharashtra, India. E-mail: amrita@iiserpune.ac.in; harinath@iiserpune.ac.in*

[b]*Department of Biology, Indian Institute of Science Education and Research Pune, Dr. Homi Bhabha Road, Pashan, Pune 411 008, Maharashtra, India*

[c]*Department of Molecular Reproduction, Development and Genetics, Indian Institute of Science, Bangalore 560012, Karnataka, India*

† Electronic supplementary information (ESI) available. See DOI: 10.1039/d1sc03828a

‡ These authors contributed equally.

§ Presently at Department of Chemistry, The Pennsylvania State University, USA.

operates by generating its own persulfide by the activation of a hyper-reactive active site cysteine with the sulfur atom of 3-mercaptopyruvate (3-MP) and produces pyruvate as the byproduct (Fig. 1A).[15] The persulfidated 3-MST (3-MST-SS$^-$) can transfer the sulfur to low molecular weight thiols such as glutathione (GSH) to produce a persulfide (GSSH), which in turn persulfidates proteins (Fig. 1B).[16] Alternately, 3-MST-SS$^-$ can produce a polysulfide species (3-MST-S$_n$S$^-$) which subsequently persulfidates low molecular weight thiols and other proteins in the cell.[2] 3-MST-SS$^-$ has been found to be involved in mitochondrial respiration and fatty acid metabolism,[17,18] synthesis of thiouridine in tRNA,[19] iron–sulfur cluster formation,[20] and in cyanide detoxification.[21] Also, 3-MST is among the major H_2S-generating enzymes in the brain and is thus implicated in regulation of the sulfane sulfur pool and sulfur trafficking in neuronal cells.[14] Therefore, a methodology that generates 3-MST-SS$^-$ in a specific, controlled and catalytic manner would be advantageous for understanding the mechanisms of sulfur metabolism, and its role in signaling and disease.

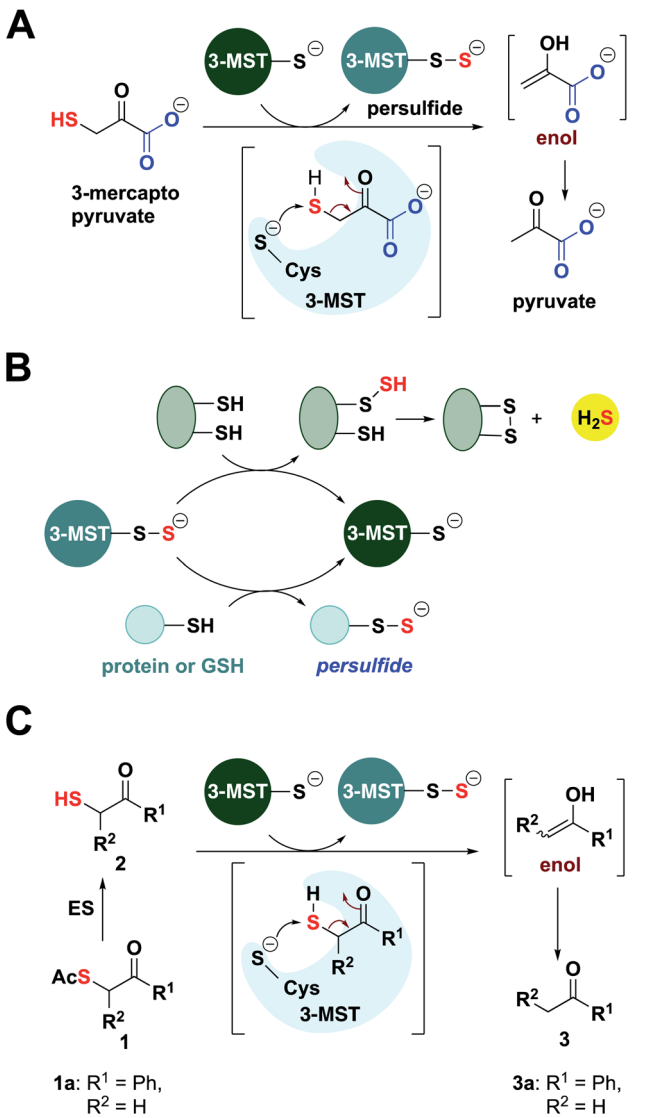

Fig. 1 (A) Catalytic cycle of 3-MST: the sulfur of 3-MP is transferred to 3-MST to produce 3-MST-SS$^-$ and pyruvate. (B) 3-MST-SS$^-$ reacts with reducing agents containing two cysteine residues such as thioredoxin (Trx) to generate H_2S. 3-MST-SS$^-$ can also generate a protein persulfide through protein–protein interaction or transfer sulfur to low molecular weight thiols such as GSH to produce glutathione persulfide (GSSH). (C) Thioacetate **1** is expected to be cleaved by esterase (ES) to produce the designed 3-MST substrate **2**. This thiol is positioned to undergo a sulfur transfer reaction to produce 3-MST-SS$^-$ and a ketone **3** as the byproduct.

The natural substrate 3-MP can, in principle, be used for this purpose. However, previous reports suggest that 3-MP produces H_2S even in the absence of 3-MST in the cell, thus, using it may have limitations.[22] Hence, our strategy of developing a suite of artificial substrates specific for 3-MST as a methodology for the controlled generation of its persulfide is unique with diverse implications. Since cellular signaling is highly dependent on the concentration and rate of generation of the signaling species, it is important that the new methodology developed contains in-built characteristics for tuning these parameters. We expect that the systematic functionalization of the artificial substrates will alter their binding to the enzyme, as well as the rate of persulfide generation (Fig. 1C). Together, these factors will consequently allow for tuning the sulfur transfer reaction. Finally, since thiols are prone to oxidation, it was envisaged that the unnatural substrate could be generated *in situ* from the corresponding thioesters through ester hydrolysis that is catalyzed by a widely prevalent esterase enzyme (Fig. 1C).

Results and discussions

Docking studies, synthesis, enzymology, detection of persulfide and H_2S

Molecular docking studies of the crystal structure of the human homolog of 3-MST (*h*3-MST, PDB ID: 4JGT) with the natural substrate 3-MP were conducted (Fig. 2A). The most energetically favorable conformation (-4.2 kcal mol^{-1}) revealed interactions with arginine residues R188 and R197 that are consistent with previous accounts of these residues aiding in anchoring the substrate carboxylate and carbonyl groups.[23,24] The cysteine C248 residue was proximal to the reactive sulfhydryl group of 3-MP at a distance of 4.4 Å.

When a similar study was conducted with the proposed aryl substrate, this compound **2a** (R^1 = Ph, R^2 = H in Fig. 1C) was well accommodated in the active site and key interactions of **2a** with R188 and R197 were preserved (Fig. 2B). The distance between the C248 and the sulfur of **2a** was 5.2 Å, which was comparable with the lowest energy conformation of 3-MP in the active site of 3-MST. The binding energy of **2a** was nearly identical with 3-MP, -4.2 kcal mol^{-1}.

We cloned and purified *h*3-MST and a bacterial 3-MST (*b*3-MST) from *Escherichia coli* (Table S3, Fig. S1†) for subsequent *in vitro* assays.[23,25] Compound **1a** (Fig. 1C) was synthesized by the treatment of 2-bromoacetophenone with potassium thioacetate using a reported protocol.[26] This compound should produce the thiol **2a** upon reaction with an esterase enzyme (ES). Compound **1a** was incubated in the presence of ES and *h*3-MST enzymes.

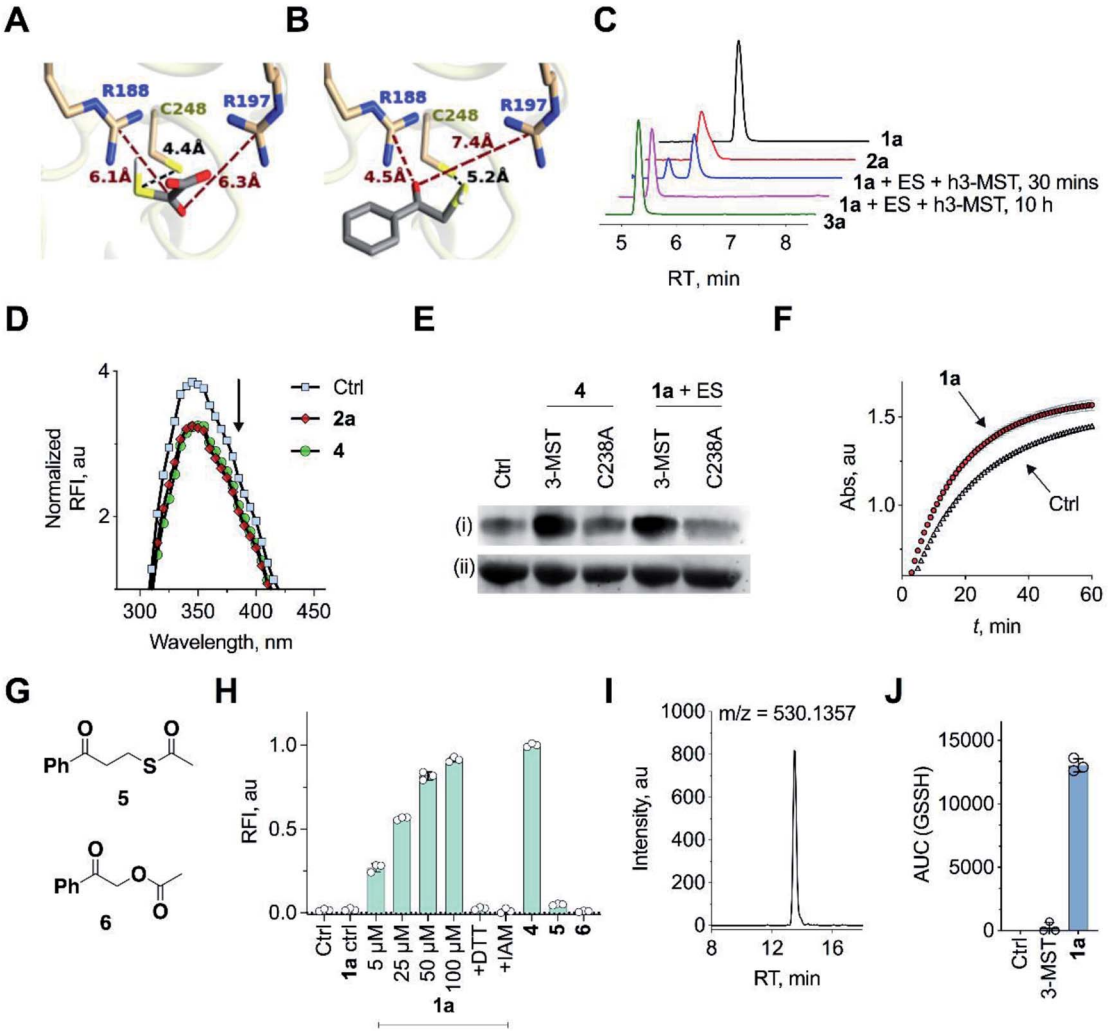

Fig. 2 (A) Docking analysis of the active site of *h*3-MST with 3-MP shows a favorable conformation with the S–S bond distance as 4.4 Å. The R188 residue is 6.1 Å from the carboxyl group whereas the R197 residue is at a distance of 6.3 Å from the carbonyl group. (B) Docking analysis of the designed substrate **2a** (R^1 = Ph, R^2 = H in Fig. 1C) reveals a similar anchoring of the substrate by the two arginine residues and the S–S bond distance was found as 5.2 Å. (C) HPLC analysis of **1a** + ES in the presence of *h*3-MST shows the formation of the thiol **2a** which is then subsequently converted to acetophenone **3a** during 10 h. (D) Intrinsic fluorescence assay on 3-MST with dimer of ethyl 3-mercaptopyruvate (E3-MP) **4** shows a decrease in fluorescence intensity which is consistent with the generation of 3-MST-SS^-. A similar result was observed with the unnatural substrate **2a**. Ctrl refers to 3-MST alone. (E) Detection of 3-MST-SS^- using the modified tag-switch technique (Fig. S7a†), conducted with **4** and **1a** + ES; The C238A 3-MST mutant treated under similar conditions showed a diminished band corresponding to the formation of 3-MST-SS^-: (i) detection of 3-MST persulfide (ii) loading control. (F) Effect of persulfidation on the activity of GAPDH: GAPDH upon treatment with **1a** + ES + 3-MST enhances its activity compared to GAPDH alone presumably due to the formation of the persulfide of GAPDH. Ctrl refers GAPDH + ES + 3-MST; **1a** refers to co-incubation of **1a** + ES + 3-MST followed by addition of GAPDH (absorbance 340 nm). (G) Structures of compounds **5** and **6**. (H) Persulfide/polysulfide detection using SSP-2: Ctrl refers to 3-MST alone and **1a** ctrl refers to **1a** + ES only (100 μM); **1a** refers to co-incubation of varying concentrations of **1a**, ES and 3-MST; +DTT: addition of DTT; +IAM: addition of iodoacetamide, an electrophile that reacts with thiols; **4** refers to incubation of the compound with 3-MST; **5** and **6** refers to the incubation of the compounds with ES followed by treatment with 3-MST. (I) Extracted ion chromatogram from a mass spectrometry-based analysis of reaction products formed upon incubation of **1a** and 3-MST in the presence of ES followed by addition of GSH as the thiol acceptor. Reaction of the reactive sulfur species (GSSH) with an electrophile monobromobimane (mBBr) was employed. LC/MS analysis revealed the formation of the GSS-bimane adduct (expected *m*/*z* = 530.1379; observed *m*/*z* = 530.1357) when **1a** was incubated with ES and 3-MST. (J) Area under the curve (AUC) for the peak corresponding to GSS-bimane (Fig. 2I); Ctrl refers to **1a** alone while 3-MST refers to 3-MST alone and **1a** refers to **1a** + ES + 3-MST.

Gradual disappearance of **1a** and concomitant formation of the thiol **2a** was observed (Fig. 2C and S2†). After 10 hours, complete disappearance of **2a** along with the formation of acetophenone **3a** was recorded. These observations suggest that after **1a** produces **2a** upon ester hydrolysis, it is utilized by 3-MST to produce **3a**. Under the same conditions, *b*3-MST also shows complete conversion to **3a** in 2 h (Fig. S3†).

The next series of experiments were designed to probe the intermediates during this transformation. The first intermediate that is expected to be formed in this reaction is 3-MST-SS^-.

The formation of 3-MST-SS$^-$ was monitored by measurement of the intrinsic fluorescence of this enzyme using a reported protocol.[27] Upon incubation of 3-MST with **2a**, a significant quenching of intrinsic fluorescence of the enzyme as compared to the apo-protein was observed suggesting the formation of 3-MST-SS$^-$ (Fig. 2D and S4†).

Compound **4**, which exists as a dimer and dissociates in buffer to produce the ethyl 3-mercaptopyruvate, E3-MP, was synthesized and used as a substrate for 3-MST (Scheme 1).[21] Molecular docking analysis gave a binding energy for this ester as −4.2 kcal mol^{-1} (Table S4†), identical to that of 3-MP. When 3-MST was incubated with 4, quenching of fluorescence was observed as before supporting the generation of the protein persulfide (Fig. 2D and S4†). A similar set of results was also recorded for *h*3-MST (Fig. S5†). The compounds themselves did not show significant fluorescence under these conditions (Fig. S6†).

A reported tag-switch assay (Fig. S7†) was used for detecting persulfidated proteins (Fig. 2E).[28] When 3-MST was reacted with **4** or with **1a** and ES, as expected, this assay confirmed the formation of 3-MST-SS$^-$ (Fig. 2E). In contrast, under similar conditions, the mutant of 3-MST where the catalytic cysteine was replaced with alanine (3-MST C238A) showed no significant increase in the signal corresponding to the 3-MST-SS$^-$ (Fig. 2E and S7†). This result is consistent with a previous report of a similar lack of activity of the *h*3-MST cysteine mutant.[29]

Next, we assayed the ability of the 3-MST-SS$^-$ to transfer the sulfide to another protein. GAPDH is a redox-sensitive protein involved in the glycolytic cycle whose active site cysteine residue is susceptible to redox fluctuations and its function is influenced by this modification.[30] Accordingly, 3-MST-SS$^-$ was prepared by treating 3-MST with **1a** in presence of ES, following which GAPDH was added and incubated for 30 min. The activity of the enzyme was then estimated using a previously reported protocol.[9] Under these conditions, the GAPDH activity was found to be significantly enhanced as compared to a GAPDH only control (Fig. 2F, S8a). Treatment with dithiothreitol (DTT), which is expected to cleave the persulfide and produce the native enzyme, resulted in an activity profile that was comparable with the control GAPDH (Fig. S8b†). Thus, 3-MST-SS$^-$, through sulfur trafficking, regulates the activity of key enzymes such as GAPDH.

The formation of persulfide/polysulfide was then assessed using SSP-2, a fluorescence turn-on probe that is sensitive to these species.[31] The probe was validated using GS$_n$SH (prepared using a reported protocol) (Fig. S9†).[10] When exposed to **1a** + ES, a distinct increase in fluorescence was recorded (Fig. 2H and S10a†). When the standard reaction mixture was treated with the reducing agent DTT, a decrease in signal, likely due to the cleavage of persulfide by DTT, was observed (Fig. 2H and S10b†). Pre-treatment with iodoacetamide (IAM), a thiol alkylating agent, is expected to inactivate the enzyme. When IAM-pre-treated 3-MST was reacted with **1a** + ES, nearly complete abrogation of signal attributable to persulfide/polysulfide generation was observed (Fig. 2H). This result is consistent with the previous observation in the tag-switch persulfide assay where we found no evidence for persulfide generation in the catalytically dead 3-MST C238A mutant. Notably, compound **4** generated persulfide at levels comparable with **1a** (Fig. S11†). Next, two control compounds – **5**, the thioacetate with an additional methylene group and **6**, the analogous ester where sulfur was replaced with oxygen – were prepared (Fig. 2G). Both these analogues should not produce persulfide under the standard assay conditions. Generation of persulfide was assessed by the tag-switch assay (Fig. S12†) as well as by the fluorescence turn-on assay and no evidence for generation of persulfide from **5** or **6** was found (Fig. 2H).

The formation of persulfide/polysulfide was next studied by leveraging the ability of 3-MST-SS$^-$ to transfer its sulfane sulfur to an acceptor thiol. GSH, a thiol found abundantly in biological systems, was reacted with the 3-MST-SS$^-$ formed from the reaction of **1a** + ES with 3-MST. The formation of various reactive sulfur species was analysed using LC/MS, where monobromobimane was used as an alkylating agent (Scheme S4†).[10] LC/MS analysis showed the formation of the GSS-bimane adduct only in the presence of **1a** + ES and 3-MST (Fig. 2I, J and S13†). In addition, we found evidence for the formation of GSSSG and H_2S as its bis-S-bimane adduct (Fig. S14 and S15†). Together, these data support the ability of our unnatural substrate–enzyme system to transfer S to low molecular weight thiols.

A standard methylene blue colorimetric assay for the detection of H_2S was conducted in the presence of DTT (Fig. 1B).[23,32] This assay revealed the formation of H_2S during incubation of **1a** with 3-MST in the presence of DTT (Fig. 3A). H_2S release from compound **4** when treated with 3-MST was also observed (Fig. S16†). Based on our observation that the thioacetate **1a** could be cleaved by DTT even in the absence of the esterase to produce **2a**, the remaining experiments were conducted with **1a** + 3-MST + DTT (Fig. S17†). The rate constant k_h for H_2S generation from **1a** when treated with *h*3-MST in the presence of DTT was 1.48 h^{-1} (Table 1). A similar rate constant k_b was observed with *b*3-MST (Table 1).

Having established that the substrates we designed could be used to generate persulfides as well as H_2S *in vitro*, their ability to permeate cells to function as substrates for cellular 3-MST was studied. A human lung carcinoma A549 cell line with 3-MST knocked down (3-MST KD) was first generated (Fig. S18†). This cell line was used in conjunction with the corresponding scrambled cell line where 3-MST levels are not perturbed (Fig. S18†). When treated with an esterase-activated H_2S donor[32] (Fig. S19†), significant enhancement in H_2S levels in both these cell lines was observed as measured by the H_2S-sensitive dye NBD-fluorescein (Fig. 3B).[33] However, in the presence of **1a**,

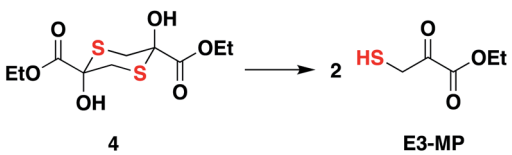

4 E3-MP

Scheme 1 Compound **4** is the dimer of E3-MP and in pH 7.4 buffer, dissociates to produce the E3-MP.

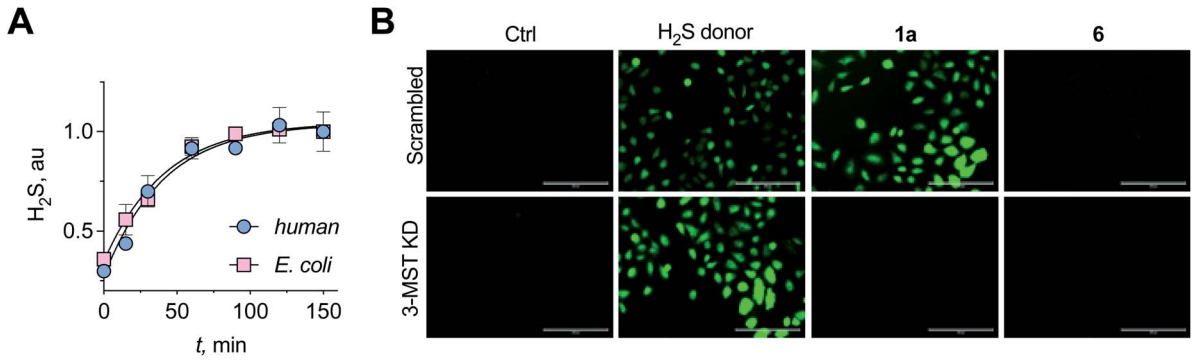

Fig. 3 (A) A methylene blue assay was used to measure the rate of H_2S generation with **1a** in the presence of *h*3-MST or *b*3-MST and DTT as the reducing agent. Nearly identical rates of H_2S generation were observed. (B) 3-MST KD refers to knock-down of expression of 3-MST in A549 cells while scrambled refers to A549 cells containing non-targeting scrambled shRNA. The H_2S donor used is an esterase-sensitive COS/H_2S donor that has been previously characterized. H_2S levels were assessed using a previously reported dye NBD-fluorescein (see ESI, Fig. S20†). Ctrl refers to untreated cells. Scale bar represents 200 μm.

Table 1 Kinetics of H_2S generation[a]

			*h*3-MST		*b*3-MST	
Compd	X	Y	k_h (h^{-1})	Rel. rate[b]	k_b (h^{-1})	k_b/k_h
1a	H	H	1.48	30	1.45	1.0
1b	NO_2	H	11.13	223	9.27	0.8
1c	CN	H	2.5	50	4.9	2.0
1d	CF_3	H	7.51	150	5.83	0.8
1e	OCF_3	H	4.48	90	2.29	0.5
1f	F	H	1.11	22	1.54	1.4
1g	Me	H	1.02	20	0.97	1.0
1h	OMe	H	0.39	8	0.37	0.9
1i	H	F	1.68	34	3.85	2.5
1j	H	OMe	0.08	2	0.99	12.5
1k	H	Me	0.05	1	1.22	25.0
1l	R^1 = Ph; R^2 = Me		Slow	—	0.19	—
1m	R^1 = 1-naphthyl; R^2 = H		0.23	5	2.87	12.5
1n	R^1 = 2-naphthyl; R^2 = H		0.50	10	1.98	4.0

[a] Reaction conditions: compound + 3-MST + DTT. H_2S was monitored using a methylene blue assay. [b] Calculated based on normalizing the rate constant with respect to **1k**.

when the 3-MST KD cells were imaged, a significantly diminished signal for intracellular H_2S levels was observed (Fig. 3B). In the scrambled cell line, however, where endogenous 3-MST levels are not perturbed, an enhanced signal corresponding to intracellular H_2S was seen (Fig. 3B). Compound **6**, which lacks a sulfur, failed to enhance H_2S in both cell lines (Fig. 3B, S20 and S21†). Together, these data suggest that **1a** is a cell-permeable persulfidating agent that is activated by 3-MST within cells to produce H_2S, putatively *via* an intracellular persulfidation mechanism, as confirmed by a separate tag-switch fluorescence reporter technique[34] (Fig. S22†).

Based on the above observations, we put forth the following mechanism for persulfide generation from this unnatural substrate – 3-MST system (Scheme 2). Cleavage of **1a** by esterase produces the thiol **2a**, which then reacts with 3-MST to produce the 3-MST-SS^- and an enol(ate), which is expected to tautomerize to the ketone **3a**. In the absence of a reducing agent, 3-MST-SS^- appears to catalyze the turnover of **2a** to produce **3a** and produces polysulfide during this transformation (Schemes 2 and S5; Fig. S15†). Under reducing conditions (DTT), 3-MST-SS^- is cleaved to produce H_2S (Scheme 2, Fig. 3A). HPLC analysis of the reaction mixture containing **2a**, 3-MST and DTT showed gradual disappearance of **2a** and the rate constant k_1 was found to be 0.99 h^{-1}. The formation of **3a** was observed and a rate constant k_2 of 0.75 h^{-1} was obtained (Fig. 4A and S23†). The rate of disappearance of **2a** and formation of **3a** was nearly identical and both parameters are comparable with the rate of H_2S generation under these conditions (Table 1, see *h*3-MST data). In the absence of 3-MST, compound **2a** is prone to oxidation to its disulfide $PhCOCH_2S$–SCH_2COPh under ambient aerobic conditions (Fig. S24†). The conversion of **1a** to **2a** (and its disulfide) occurs in a nearly quantitative yield. Hence, our overall analysis demonstrates that compound **1a** is an excellent substrate for 3-MST and produces a persulfide intermediate, which is cleaved under reducing conditions to produce H_2S. In the absence of esterase, **1a** is gradually consumed in the presence of 3-MST and the formation of **3a** is observed after several hours (Fig. S25 and S26†). Also, persulfide/polysulfide were detected using the probe SSP-2 under similar conditions (Fig. S27†). We find no evidence for the formation of the thiol **2a**. This may be explained by the formation of 3-MST thioacetate as a possible intermediate during the transformation of **1a** to **3a** (Scheme S5†).

Substrate scope

In order to assess the unnatural substrate scope and the possibility of tuning sulfur transfer using this newly developed

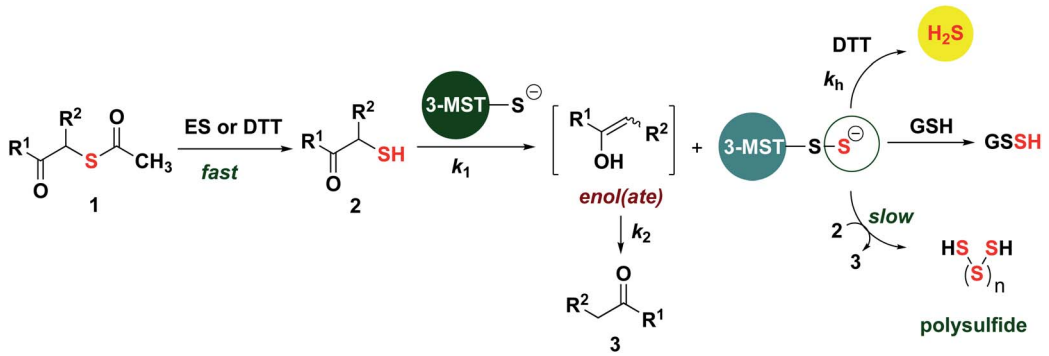

Scheme 2 Proposed mechanism: thioacetate **1** is cleaved by esterase or DTT (HPLC in Fig. S23, ESI†) to produce the thiol **2**, which is then turned over by 3-MST to produce 3-MST-SS$^-$ and an enol(ate). The enol(ate) in aqueous buffer is rapidly converted to the ketone **3**. 3-MST-SS$^-$ in the presence of a reducing agent produces H_2S. 3-MST-SS$^-$ can react with low molecular weight thiols such as GSH to produce GSSH. Under non-reducing conditions, 3-MST-SS$^-$ can further turn over **2**, generating the ketone **3**; the likely byproduct of this reaction is polysulfide.

protocol, we synthesized a series of analogues. Arginine residues in the active site interact with the carbonyl group of 3-MP and are implicated in stabilizing the pyruvate enolate.[23,24,27] In order to test if the stability of the incipient enolate played a role in the rates of H_2S production, compounds **1b–1h** with electron-withdrawing or electron-donating groups were synthesized. Molecular docking analysis with the corresponding thiols **2b–2h** showed nearly identical conformations (Table S5†). The rate constants of H_2S release ranged from 0.39 to 7.51 h^{-1} (Table 1, Fig. S28†). Hammett analysis of rate constants gave a positive ρ value of +1.11, that is consistent with a partial negative charge developing in the transition state in the rate limiting step of the reaction (Fig. 4B).

Due to the proximity of a substituent at the *ortho* position of the aryl ring, enolate formation is likely to be affected by stereoelectronic effects. In order to investigate these effects, compounds **1i–1k** were prepared and their H_2S release was recorded (Table 1, Fig. S29†). While the rate of H_2S release from **1i** was comparable with **1a**, compounds **1j** and **1k** were substantially slower in generating H_2S when compared with **1a**. Molecular docking studies with the 2-fluorophenyl derivative **2i** showed a conformation and S–S distance comparable with that of **2a** bound to the active site (Table S6†). However, the lowest energy conformation of the thiol **2k** was significantly removed from the active site with the S–S bond distance of 10.7 Å (Fig. 4C). Unlike **2a**, the interaction of **2k** with the active site cysteine is restricted by steric clashes of A185 and R188 with its *ortho*-Me group, as illustrated in a higher energy conformation (Fig. 4D). A similar result was recorded for the 2-methoxy derivative **2j** (Tables S6 and S7†). These studies provide a molecular basis for the diminished H_2S release rates from these analogues.

In addition to electronics, enolate stability and reactivity can also be affected by sterics. In order to study the effects of an added substituent, compound **1l** which has an α-methyl substituent was synthesized. Docking analysis of **2l** with 3-MST revealed a docking score as well as a conformation that was comparable with **2a** (Table S6†). H_2S release from **1l** was, however, found to be extremely slow (Table 1, Fig. S30†). The formation of the enolate appears to be more sensitive to steric effects than electronic effects. Recently, inhibitors for 3-MST were developed and one of these inhibitors had a naphthyl ring.[35] Taking this cue, compounds **1m** and **1n** were synthesized (Table S2†). Our assays confirmed that these compounds were substrates for 3-MST, and H_2S generation rates were moderately higher when compared with **1a** (Table 1, Fig. S30†) suggesting that a combination of binding and turnover is essential for tuning 3-MST-mediated sulfur transfer reactions.

Normalizing the rate constants with respect to **1k** revealed more than a 100-fold difference in relative rates for H_2S release (Table 1). This observation suggests that this series of substrates can be used to tune rates of persulfide/polysulfide generation. Next, bacterial 3-MST was used to study the rates of H_2S generation from the analogues and first-order rate constants were calculated (Table 1). Linear free energy relationship study of H_2S generation rates of **1a–1h** with *b*3-MST gave a slope of +1.13 (Fig. S31†), comparable with the data from *h*3-MST. Control compounds **5** and **6** do not produce H_2S under these conditions, as expected (Fig. S32†). Under the standard reaction conditions with 3-MST homologs, we found no major difference in rates of H_2S release from **4** (Fig. S16†). While a majority of the substrates tested showed similar rates, compounds **1j**, **1k** and **1m** whose $k_b/k_h > 10$, were notable exceptions. These results indicate that our approach differentiates between human and bacterial 3-MST homologs, and is capable of achieving selective H_2S generation between species. To the best of our knowledge, this is the first example of tuning persulfide/polysulfide generation, with the added advantage of species selectivity.

Antioxidant activity

Persulfides are widely prevalent in cells as protein persulfides as well as other low molecular weight persulfide species. For example, glutathione persulfide/polysulfide has excellent *in vitro* ROS-scavenging activity when compared with glutathione or H_2S alone.[10] These species have been previously shown to have potent antioxidant activity likely through the Nrf2-KEAP1 pathway, imparting protection from ROS-induced injury.[36,37] Selected analogues with varying relative rates of H_2S generation

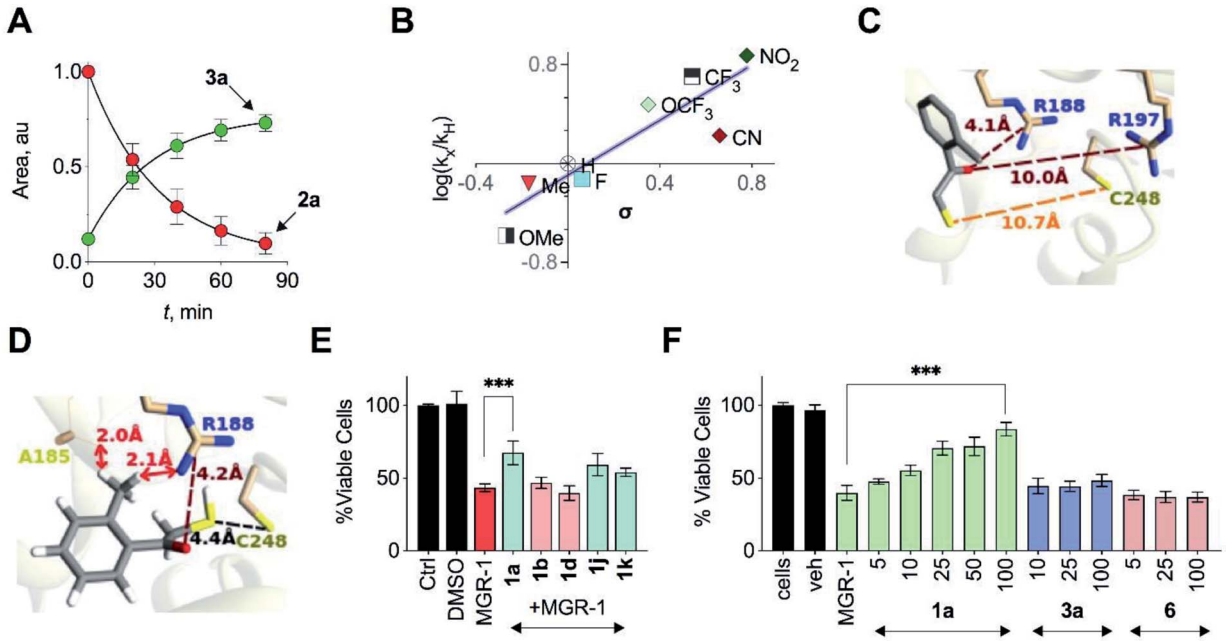

Fig. 4 (A) HPLC analysis of a reaction mixture containing **2a** and 3-MST in the presence of DTT showed the gradual disappearance of **2a** and concomitant formation of **3a**. Curve fitting to first order kinetics gave rate constants of 0.99 h^{-1} and 0.75 h^{-1} for the disappearance of **2a** and the formation of **3a**, respectively. (B) Hammett analysis of rate constants of H_2S generation from unnatural substrates (see Table 1) with wt *h*3-MST. Linear regression analysis yielded a slope of +1.11 ($R^2 = 0.8$). (C) Docking of **2k** in the active site of *h*3-MST shows S–S bond distance of 10.7 Å which is substantially larger when compared with the low energy conformation of **2a** (5.2 Å). (D) Docking of **2k** in the active site of *h*3-MST shows steric clashes of ortho-Me group of **2k** with A185 and R188 residues in a higher energy conformation. (E) Cell viability assay conducted on N2a cells: Cells were pre-treated with 25 μM of compounds **1a**, **1b**, **1d**, **1j** and **1k** for 12 h and then exposed to MGR-1 (25 μM) for 4 h. Ctrl refers to untreated cells. Cell viability was determined using a standard MTT assay. Results are expressed as mean ± SD ($n = 3$). ***$p < 0.001$ *vs.* MGR-1. (F) Cell viability assay conducted on N2a cells: cells that were pre-treated with **1a**, **3a** or **6** were then treated with a cell permeable ROS generator MGR-1. A dose-dependent protection of cells from MGR-1 induced cell death by **1a** was observed. The byproduct ketone **3a** or the negative control **6** did not show any protection against the cytotoxic effects of MGR-1. All data are presented as mean ± SD ($n = 3$ per group). ***$p < 0.001$ *vs.* MGR-1.

(in the range of 1 to 223) were next tested to study their protective ability against oxidative stress-induced cell death. A mouse neuroblastoma cell line N2a was used in this experiment. MGR-1, a known cell-permeable ROS generator, was used to induce oxidative stress and cell viability was determined.[38] N2a cells were first independently treated with fast H_2S generators **1b** and **1d** (relative rate > 50), **1a** (relative rate = 30) as well as slow generators **1j** and **1k** (relative rate < 2). At 25 μM, these compounds showed no significant effect on the growth of cells as determined by a cell viability assay (Fig. S33†). Cells that were independently pre-incubated with these compounds (25 μM) for 12 h were next exposed to MGR-1. Viable cells were determined using a standard cell viability assay. The results of this assay indicate that the fast generators did not significantly protect cells from oxidative stress-induced cell death while the other analogues **1a**, **1j** and **1k** showed remarkable protective effects (Fig. 4E). From this initial screen, we identified compound **1a** for further evaluation. The compound **1a** itself was well tolerated by cells (Fig. S34†) and the byproduct of turnover of **1a** is **3a**, which is classified as Generally Recognized as Safe (GRAS) by the Food and Drug Administration.

The lead compound **1a** was next tested against N2a cells using MGR-1, and a dose-dependent protection from lethality was recorded (Fig. 4F). The control compound **6** and the acetophenone **3a** tested under similar conditions failed to show any protective effects (Fig. 4F). To further corroborate our results, menadione, another known ROS generator was used to induce lethality. Again, a dose-dependent protection was recorded when cells were pre-treated with **1a** (Fig. S35†). In a separate experiment with mouse embryonic fibroblasts (MEF), **1a** was similarly found to have significant protective effects (Fig. S36†). Together, these data illustrate the cytoprotective effect of the cell-permeable persulfide generator **1a**.

To validate the molecular basis of this result, the effect of **1a** in reducing hydrogen peroxide (H_2O_2) levels in cells was studied. Again, MGR-1 was used to increase H_2O_2 as determined by the TCF-B fluorescent dye in A549 cells (Fig. 5A).[39] When cells pre-treated with **1a** were exposed to MGR-1, a significant decrease in H_2O_2 levels was observed (Fig. 5A). Under similar conditions, control compound **6** did not affect H_2O_2 levels in cells, suggesting that the ROS-quenching effects were directly mediated by persulfide/H_2S generated by **1a** (Fig. S37†).

Elevation of ROS in cells leads to perturbation of redox homeostasis and alteration of levels of various components of cellular antioxidant response. NAD^+/NADH and GSSG/GSH ratio serve as reliable markers of oxidative stress.[40] Three cell lines

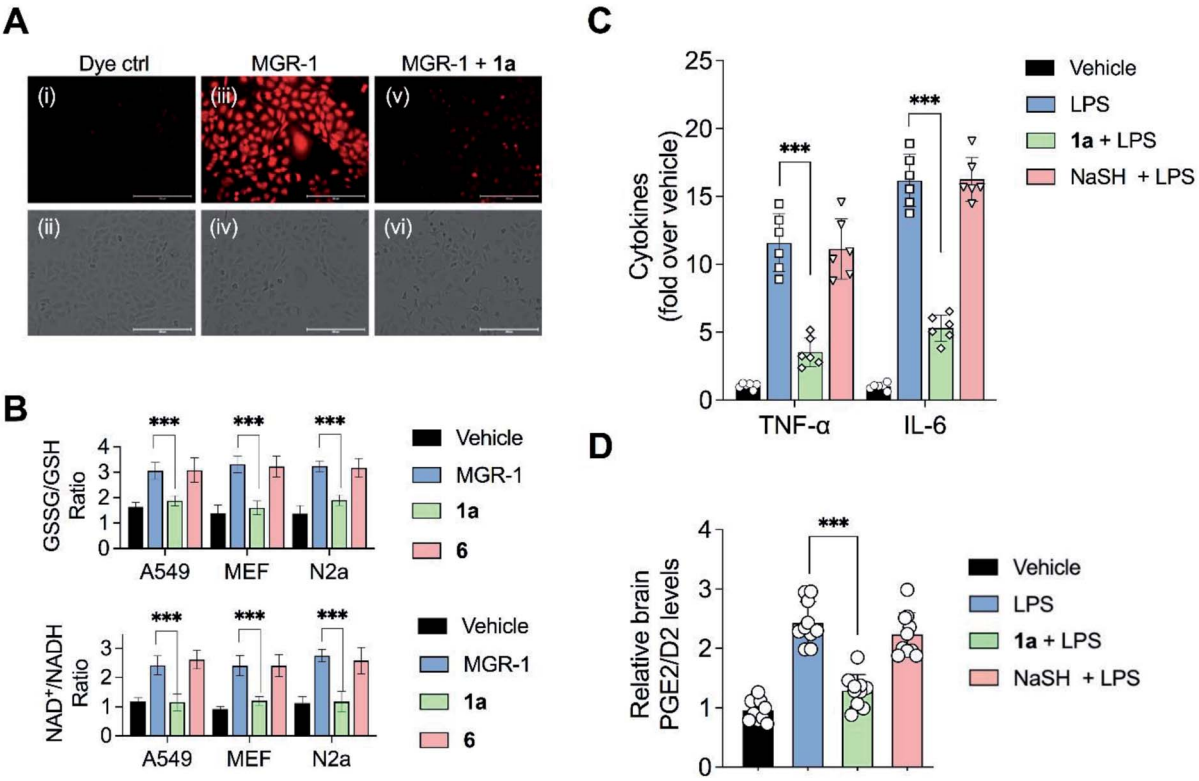

Fig. 5 (A) Effects of **1a** on quenching hydrogen peroxide (H_2O_2) generated by MGR1:A549 cells treated with: (i and ii) dye control; (iii and iv) 25 μM MGR-1; (v and vi) 25 μM of **1a** for 12 h followed by addition of the 25 μM MGR-1 for 1 h. Intracellular H_2O_2 was detected using a reported H_2O_2-sensor TCF-B (25 μM). Scale bar represents 200 μm. (B) Biomarkers for oxidative stress: Three cell lines (A549, mouse embryonic fibroblasts (MEF) and N2a) were pre-treated with vehicle, **1a** or **6** and exposed to MGR-1 following which NAD^+/NADH ratio and GSSG/GSH ratio were determined using an ELISA assay. All data are presented as mean ± SD ($n = 5$ per group). ***$p < 0.001$ *vs.* MGR-1. (C and D) Mouse endotoxin shock model: animals were treated with **1a** (20 mg kg^{-1}) or NaSH (20 mg kg^{-1}) 4 h prior to treatment with lipopolysaccharide (LPS, 5 mg kg^{-1}). 30 min post-administration of LPS, another dose of **1a** or NaSH was given. The brain tissue samples were harvested followed by measurement of: (C) Pro-inflammatory cytokines, TNF-α and IL-6 using a standard ELISA assay. All data are presented as mean ± SD ($n = 6$ per group). ***$p < 0.001$ *vs.* LPS; and (D) prostaglandins PGE2/D2 using LC/MS. All data are presented as mean ± SD ($n = 10$ per group). ***$p < 0.001$ *vs.* LPS.

(A549, MEF and N2a) were exposed to MGR-1 and enhanced NAD^+/NADH as well as GSSG/GSH ratios were recorded (Fig. 5B). Pre-treatment of cells with **1a** followed by incubation with MGR-1 showed restoration of nearly normal ratios, and the control compound **6** was found to be ineffective in doing so. Taken together, these studies conclusively establish the efficacy of the artificial substrate **1a** that we designed to mitigate oxidative stress in both human as well as mouse-derived cell lines (Fig. 5B).[35]

Mitigation of neuroinflammation

Recently, a polysulfide donor was used to study the effect of enhanced endogenous polysulfide levels on innate immune response using a mouse endotoxin shock model.[41] Lipopolysaccharides (LPS), a common constituent of bacterial cell walls, are recognized by toll-like receptor 4 (TLR4) and trigger the innate immune response leading to the activation of macrophages to generate pro-inflammatory cytokines that contribute to clearance of bacteria (Fig. S38†). The major finding of this study was that elevated polysulfides can negatively regulate TLR4-mediated pro-inflammatory signaling and the polysulfide donor protects against this endotoxin shock. Taking this cue, we evaluated the ability of **1a** to mitigate neuroinflammation in a similar mouse model system. First, C57BL/6J mice were intraperitoneally injected once daily with compound **1a** over a period of seven days, and it was found to be well tolerated. Next, mice were treated with LPS alone and increased levels of pro-inflammatory cytokines TNF-α and IL-6 in the brain were observed as compared with vehicle-treated mice (Fig. 5C).

In a separate experiment, mice which were treated with LPS and **1a** were found to have significantly lower levels of TNF-α and IL-6 in the brain, suggesting that **1a** suppressed the inflammatory response triggered by LPS. No evidence for reduction of pro-inflammatory cytokines in mice treated with LPS and NaHS was observed, consistent with the previous report that NaHS had little or no effect on the reduction of cytokines.[41] LPS is also known to induce the formation of pro-inflammatory prostaglandins in the brain. Prostaglandin E2 (PGE2) has a variety of functions in the nervous system. Interaction of PGE2 with prostaglandin EP3 receptors leads to an increase in body temperature and inflammation (Fig. S39†). The use of nonsteroidal anti-inflammatory drugs (NSAIDs) blocks the activity of cyclooxygenase-2 (COX-2) which decreases PGE2 production,

resulting in remediation of fever and inflammation.[42] Hence, measurement of PGE2/D2 levels is a reliable inflammation biomarker. LC/MS analysis of brain homogenates was carried out to measure PGE2/D2 levels. LPS-treated mice were found to have significantly higher levels of PGE2/D2 when compared with vehicle-treated mice. Animals which were exposed to both LPS and **1a** were found to have significantly lower levels of PGE2/D2, reiterating the ability of **1a** to reduce neuroinflammation (Fig. 5D). Again, NaSH-treated mice that were exposed to LPS did not show any effect on PGE2/D2 levels. Taken together, these assays conclusively demonstrate the ability of **1a** to act as an antioxidant as well as an anti-inflammatory agent.

Our data shows that the unnatural substrate is able to transfer sulfur to low molecular weight thiols *via* 3-MST, and induce protein persulfidation in cells. Other strategies for generating persulfides in cells have relied on installing the persulfide/polysulfide functional group in the donor.[5,6,41,43–53] These strategies work very well but have limitations in the ease of synthesis, poor shelf-life due to susceptibility towards decomposition, and heterogeneity of the persulfide source due to the ambiguity in the number of sulfurs in the donor. The protocol developed here involves the synthesis of a thioacetate, which is easy to prepare with high reproducibility and is stable for extended periods. For *in vitro* experiments to generate persulfide, the addition of enzymes that are readily available (esterase and 3-MST) is necessary while for cellular experiments to enhance persulfide, addition of the compound is sufficient. The substrates we have developed allow for systematic study of cellular sulfur transfer, and can be used to investigate the persulfide proteome which has been elusive till date.[11]

Conclusions

The study of reactive sulfur species is often complicated by poor detection techniques, artefacts and uncharacterized cellular interactions. Thus, several facets of sulfur metabolism remain to be studied in molecular-level detail. The use of selective tools developed herein allow for systematic study of redox biology through the lens of an important enzyme, 3-MST. Our data underscores the potential of this approach as a novel therapeutic paradigm in mitigating inflammation. The importance of persulfides in ameliorating symptoms associated with neurodegenerative disorders as well as favourably impacting behavior in animals are some of the possible applications of the strategy developed here.[4] The tunability of rates of persulfide generation using the class of compounds that we have developed adds a new dimension to persulfide donors that has hitherto not been studied. Projecting forward, further structural optimization of the substrate would be necessary to fully exploit the translational potential of this approach. The deficits associated with diminished expression of 3-MST will likely need mapping out the 3-MST-SS^- proteome and identification of proteins that depend on this enzyme for persulfidation. Given the selectivity of the substrate towards 3-MST in cells, the use of our compounds as probes for studying sulfur trafficking will provide insights into molecular mechanisms associated with the dysfunction or deficiency of 3-MST in neuronal diseases, such as intellectual disability and Down's syndrome.[54,55]

Data availability

Experimental protocols, characterization and all data pertaining to the manuscript have been uploaded in the ESI.†

Author contributions

ABH and HC wrote the manuscript with inputs from all authors. PB, SM, MN, RRMS, SS, VSSA and KG carried out the experiments and computation under the supervision of AM, DKS, SSK, ABH and HC.

Conflicts of interest

There are no conflicts to declare.

Acknowledgements

Financial support from the SERB, DST (CRG/2019/002900) and IISER Pune is acknowledged. This work was supported by the DBT-Ramalingaswami Re-entry Fellowship (grant number BT/RLF/Re-entry/12/2014) awarded to ABH. DBT/Wellcome Trust India Alliance Fellowship (grant number IA/I/15/2/502058) awarded to SSK. DST Fund for Improvement of S&T Infrastructure (SR/FST/LSII-043/2016) to the IISER Pune Biology Department for setting up the Biological Mass Spectrometry Facility. The National Facility for Gene Function in Health and Disease at IISER Pune is thanked for maintaining and providing mice for this study (DBT: BT/INF/22/SP17358/2016). Research fellowship for PB (DST-INSPIRE), SM (UGC) and RRMS (CSIR) are acknowledged. The authors thank Dr Rajesh Viswanathan, IISER Tirupati and Dr Sridhar Rajaram, JNCASR Bengaluru for their critical reading of the manuscript.

Notes and references

1 M. R. Filipovic, J. Zivanovic, B. Alvarez and R. Banerjee, *Chem. Rev.*, 2018, **118**, 1253–1337.
2 T. V. Mishanina, M. Libiad and R. Banerjee, *Nat. Chem. Biol.*, 2015, **11**, 457.
3 M. S. Vandiver, B. D. Paul, R. Xu, S. Karuppagounder, F. Rao, A. M. Snowman, H. Seok Ko, Y. Il Lee, V. L. Dawson, T. M. Dawson, N. Sen and S. H. Snyder, *Nat. Commun.*, 2013, **4**, 1626.
4 D. Giovinazzo, B. Bursac, J. I. Sbodio, S. Nalluru, T. Vignane, A. M. Snowman, L. M. Albacarys, T. W. Sedlak, R. Torregrossa, M. Whiteman, M. R. Filipovic, S. H. Snyder and B. D. Paul, *Proc. Natl. Acad. Sci. U. S. A.*, 2021, **118**, e2017225118.
5 Y. Zheng, B. Yu, Z. Li, Z. Yuan, C. L. Organ, R. K. Trivedi, S. Wang, D. J. Lefer and B. Wang, *Angew. Chem., Int. Ed.*, 2017, **56**, 11749–11753.
6 V. S. Khodade, B. M. Pharoah, N. Paolocci and J. P. Toscano, *J. Am. Chem. Soc.*, 2020, **142**, 4309–4316.

7 K. Shatalin, E. Shatalina, A. Mironov and E. Nudler, *Science*, 2011, **334**, 986–990.
8 P. Shukla, V. S. Khodade, M. SharathChandra, P. Chauhan, S. Mishra, S. Siddaramappa, B. E. Pradeep, A. Singh and H. Chakrapani, *Chem. Sci.*, 2017, **8**, 4967–4972.
9 A. K. Mustafa, M. M. Gadalla, N. Sen, S. Kim, W. Mu, S. K. Gazi, R. K. Barrow, G. Yang, R. Wang and S. H. Snyder, *Sci. Signaling*, 2009, **2**, ra72.
10 T. Ida, T. Sawa, H. Ihara, Y. Tsuchiya, Y. Watanabe, Y. Kumagai, M. Suematsu, H. Motohashi, S. Fujii, T. Matsunaga, M. Yamamoto, K. Ono, N. O. Devarie-Baez, M. Xian, J. M. Fukuto and T. Akaike, *Proc. Natl. Acad. Sci. U. S. A.*, 2014, **111**, 7606–7611.
11 J. Zivanovic, E. Kouroussis, J. B. Kohl, B. Adhikari, B. Bursac, S. Schott-Roux, D. Petrovic, J. L. Miljkovic, D. Thomas-Lopez, Y. Jung, M. Miler, S. Mitchell, V. Milosevic, J. E. Gomes, M. Benhar, B. Gonzales-Zorn, I. Ivanovic-Burmazovic, R. Torregrossa, J. R. Mitchell, M. Whiteman, G. Schwarz, S. H. Snyder, B. D. Paul, K. S. Carroll and M. R. Filipovic, *Cell Metab.*, 2019, **30**, 1152–1170.
12 N. Nagahara and A. Katayama, *J. Biol. Chem.*, 2005, **280**, 34569–34576.
13 N. Nagahara, *Br. J. Pharmacol.*, 2018, **175**, 577–589.
14 Y. Kimura, S. Koike, N. Shibuya, D. Lefer, Y. Ogasawara and H. Kimura, *Sci. Rep.*, 2017, **7**, 10459.
15 N. Nagahara and T. Nishino, *J. Biol. Chem.*, 1996, **271**, 27395–27401.
16 M. Libiad, P. K. Yadav, V. Vitvitsky, M. Martinov and R. Banerjee, *J. Biol. Chem.*, 2014, **289**, 30901–30910.
17 K. Módis, C. Coletta, K. Erdélyi, A. Papapetropoulos and C. Szabo, *FASEB J.*, 2013, **27**, 601–611.
18 M. Li, C. Xu, J. Shi, J. Ding, X. Wan, D. Chen, J. Gao, C. Li, J. Zhang, Y. Lin, Z. Tu, X. Kong, Y. Li and C. Yu, *Gut*, 2018, **67**, 2169–2180.
19 P. M. Palenchar, C. J. Buck, H. Cheng, T. J. Larson and E. G. Mueller, *J. Biol. Chem.*, 2000, **275**, 8283–8286.
20 E. G. Mueller, *Nat. Chem. Biol.*, 2006, **2**, 185.
21 H. T. Nagasawa, D. J. W. Goon, D. L. Crankshaw, R. Vince and S. E. Patterson, *J. Med. Chem.*, 2007, **50**, 6462–6464.
22 C. Coletta, K. Módis, B. Szczesny, A. Brunyánszki, G. Oláh, E. C. S. Rios, K. Yanagi, A. Ahmad, A. Papapetropoulos and C. Szabo, *Mol. Med.*, 2015, **21**, 1–14.
23 P. K. Yadav, K. Yamada, T. Chiku, M. Koutmos and R. Banerjee, *J. Biol. Chem.*, 2013, **288**, 20002–20013.
24 G.-T. Huang and J.-S. K. Yu, *J. Phys. Chem. B*, 2016, **120**, 4608–4615.
25 F. van den Ent and J. Löwe, *J. Biochem. Biophys. Methods*, 2006, **67**, 67–74.
26 A. A. Heredia, S. M. Soria-Castro, L. M. Bouchet, G. Oksdath-Mansilla, C. A. Barrionuevo, D. A. Caminos, F. R. Bisogno, J. E. Argüello and A. B. Peñéñory, *Org. Biomol. Chem.*, 2014, **12**, 6516–6526.
27 J.-C. Lec, S. Boutserin, H. Mazon, G. Mulliert, S. Boschi-Muller and F. Talfournier, *ACS Catal.*, 2018, **8**, 2049–2059.
28 D. Zhang, I. Macinkovic, N. O. Devarie-Baez, J. Pan, C.-M. Park, K. S. Carroll, M. R. Filipovic and M. Xian, *Angew. Chem., Int. Ed.*, 2014, **53**, 575–581.
29 N. Shibuya, M. Tanaka, M. Yoshida, Y. Ogasawara, T. Togawa, K. Ishii and H. Kimura, *Antioxid. Redox Signaling*, 2009, **11**, 703–714.
30 C. Tristan, N. Shahani, T. W. Sedlak and A. Sawa, *Cell. Signalling*, 2011, **23**, 317–323.
31 W. Chen, C. Liu, B. Peng, Y. Zhao, A. Pacheco and M. Xian, *Chem. Sci.*, 2013, **4**, 2892.
32 P. Chauhan, P. Bora, G. Ravikumar, S. Jos and H. Chakrapani, *Org. Lett.*, 2017, **19**, 62–65.
33 C. Wei, Q. Zhu, W. Liu, W. Chen, Z. Xi and L. Yi, *Org. Biomol. Chem.*, 2014, **12**, 479–485.
34 R. Wedmann, C. Onderka, S. Wei, I. A. Szijártó, J. L. Miljkovic, A. Mitrovic, M. Lange, S. Savitsky, P. K. Yadav, R. Torregrossa, E. G. Harrer, T. Harrer, I. Ishii, M. Gollasch, M. E. Wood, E. Galardon, M. Xian, M. Whiteman, R. Banerjee and M. R. Filipovic, *Chem. Sci.*, 2016, **7**, 3414–3426.
35 K. Hanaoka, K. Sasakura, Y. Suwanai, S. Toma-Fukai, K. Shimamoto, Y. Takano, N. Shibuya, T. Terai, T. Komatsu, T. Ueno, Y. Ogasawara, Y. Tsuchiya, Y. Watanabe, H. Kimura, C. Wang, M. Uchiyama, H. Kojima, T. Okabe, Y. Urano, T. Shimizu and T. Nagano, *Sci. Rep.*, 2017, **7**, 40227.
36 G. Yang, K. Zhao, Y. Ju, S. Mani, Q. Cao, S. Puukila, N. Khaper, L. Wu and R. Wang, *Antioxid. Redox Signaling*, 2012, **18**, 1906–1919.
37 S. Koike, Y. Ogasawara, N. Shibuya, H. Kimura and K. Ishii, *FEBS Lett.*, 2013, **587**, 3548–3555.
38 D. S. Kelkar, G. Ravikumar, N. Mehendale, S. Singh, A. Joshi, A. K. Sharma, A. Mhetre, A. Rajendran, H. Chakrapani and S. S. Kamat, *Nat. Chem. Biol.*, 2019, **15**, 169–178.
39 A. C. Sedgwick, H.-H. Han, J. E. Gardiner, S. D. Bull, X.-P. He and T. D. James, *Chem. Commun.*, 2017, **53**, 12822–12825.
40 F. Q. Schafer and G. R. Buettner, *Free Radical Biol. Med.*, 2001, **30**, 1191–1212.
41 T. Zhang, K. Ono, H. Tsutsuki, H. Ihara, W. Islam, T. Akaike and T. Sawa, *Cell Chem. Biol.*, 2019, **26**, 686–698.
42 J. R. Vane, *Nat. New Biol.*, 1971, **231**, 232–235.
43 P. Bora, P. Chauhan, S. Manna and H. Chakrapani, *Org. Lett.*, 2018, **20**, 7916–7920.
44 A. Chaudhuri, Y. Venkatesh, J. Das, M. Gangopadhyay, T. K. Maiti and N. D. P. Singh, *J. Org. Chem.*, 2019, **84**, 11441–11449.
45 R. A. Hankins, S. I. Suarez, M. A. Kalk, N. M. Green, M. N. Harty and J. C. Lukesh, *Angew. Chem.*, 2020, **132**, 22422–22429.
46 V. S. Khodade, S. C. Aggarwal, B. M. Pharoah, N. Paolocci and J. P. Toscano, *Chem. Sci.*, 2021, **12**, 8252–8259.
47 B. Yu, Y. Zheng, Z. Yuan, S. Li, H. Zhu, L. K. De La Cruz, J. Zhang, K. Ji, S. Wang and B. Wang, *J. Am. Chem. Soc.*, 2018, **140**, 30–33.
48 Z. Yuan, Y. Zheng, B. Yu, S. Wang, X. Yang and B. Wang, *Org. Lett.*, 2018, **20**, 6364–6367.
49 J. Kang, S. Xu, M. N. Radford, W. Zhang, S. S. Kelly, J. J. Day and M. Xian, *Angew. Chem., Int. Ed.*, 2018, **57**, 5893–5897.
50 C. R. Powell, M. K. Dillon, Y. Wang, R. J. Carrazzone and J. B. Matson, *Angew. Chem., Int. Ed.*, 2018, **57**, 6324–6328.

51 K. M. Dillon, R. J. Carrazzone, Y. Wang, C. R. Powell and J. B. Matson, *ACS Macro Lett.*, 2020, **9**, 606–612.
52 Y. Wang, K. M. Dillon, Z. Li, E. W. Winckler and J. B. Matson, *Angew. Chem., Int. Ed.*, 2020, **59**, 16698–16704.
53 V. S. Khodade and J. P. Toscano, *J. Am. Chem. Soc.*, 2018, **140**, 17333–17337.
54 Y. Suwanai, N. Nagahara, Z. Naito and H. Orimo, *Adv. Tech. Biol. Med.*, 2016, **4**, 167.
55 T. Panagaki, E. B. Randi and C. Szabo, *Biomolecules*, 2020, **10**, 653.